Spatio-temporal Analysis of Molecular Determinants of Neuronal Degeneration in the Aging Mouse Cerebellum*[S]

Erik L. de Graaf‡§¶, Wilbert P. Vermeij¶‖, Monique C. de Waard¶‖**, Yvonne Rijksen¶‖**, Ingrid van der Pluijm¶‖**, Casper C. Hoogenraad‡‡, Jan H. J. Hoeijmakers¶‖**, A. F. Maarten Altelaar‡§ §§, and Albert J. R. Heck‡§¶§§**

The accumulation of cellular damage, including DNA damage, is hypothesized to contribute to aging-related neurodegenerative changes. DNA excision repair cross-complementing group 1 (Ercc1) knock-out mice represent an accepted model of neuronal aging, showing gradual neurodegenerative changes, including loss of synaptic contacts and cell body shrinkage. Here, we used the Purkinje cell-specific *Ercc1* DNA-repair knock-out mouse model to study aging in the mouse cerebellum. We performed an in-depth quantitative proteomics analysis, using stable isotope dimethyl labeling, to decipher changes in protein expression between the early (8 weeks), intermediate (16 weeks), and late (26 weeks) stages of the phenotypically aging *Ercc1* knock-out and healthy littermate control mice. The expression of over 5,200 proteins from the cerebellum was compared quantitatively, whereby 79 proteins (*i.e.* 1.5%) were found to be substantially regulated during aging. Nearly all of these molecular markers of the early aging onset belonged to a strongly interconnected network involved in excitatory synaptic signaling. Using immunohistological staining, we obtained temporal and spatial profiles of these markers confirming not only the proteomics data but in addition revealed how the change in protein expression correlates to synaptic changes in the cerebellum. In summary, this study provides a highly comprehensive spatial and temporal view of the dynamic changes in the cerebellum and Purkinje cell signaling in particular, indicating that synapse signaling is one of the first processes to be affected in this premature aging model, leading to neuron morphological changes, neuron degeneration, inflammation, and ultimately behavior disorders. ***Molecular & Cellular Proteomics 12: 10.1074/mcp.M112.024950, 1350–1362, 2013.***

A link between DNA damage and the process of aging has been firmly established (1, 2). The brain in particular is a vulnerable organ that is plagued by various neurodegenerative disorders that have been related to aging, *i.e.* Alzheimer and Parkinson disease. The study of the early onset of age-related neurodegenerative diseases is challenging, because there are not many confident early molecular determinants that predict their development. Therefore, progeroid syndromes (showing premature aging) are often used as a model for segmental aging as they show consistent and predictive elements of the aging phenotype (*e.g.* cessation of growth and development, hearing loss, and severe and progressive neuron dysfunction) (1, 3). These accelerated aging syndromes have in common that they carry defects in one or multiple proteins involved in DNA damage repair mechanisms.

A well established progeroid mouse model is the excision repair cross-complementing group 1 (Ercc1)[1] gene knock-out (4, 5). The Ercc1-xeroderma pigmentosum group F complex acts as a nuclease in the nucleotide excision repair pathway and has an important function in both global genome and transcription-coupled DNA damage repair. Besides its role in nucleotide excision repair, Ercc1 is also involved in interstrand cross-link repair and oxidative damage repair. The accumulation of DNA damage following *Ercc1* gene inactivation results in the progeroid phenotype (2, 6). Recently, it was shown that global and neuron-specific *Ercc1* mutant mice showed age-related neuronal changes in the spinal cord and the hippocampus (7, 8). Here, we set out to monitor molecular changes in the cerebellum of Purkinje cell-specific Ercc1 knock-out mice by quantitative proteomics. The advantage of a cell type-specific knock-out, over a global knock-out, is that the organism is not compromised by secondary side effects

From the ‡Biomolecular Mass Spectrometry and Proteomics Group, Utrecht Institute for Pharmaceutical Sciences and Bijvoet Center for Biomolecular Research, Utrecht University, Padualaan 8, 3584 CH Utrecht, the §Netherlands Proteomics Centre, Padualaan 8, 3584 CH Utrecht, the ¶Center for Biomedical Genetics, ‖Department of Genetics, Erasmus Medical Centre, postal code: 3015 GE Rotterdam, and the **Cancer Genomics Centre and ‡‡Cell Biology, Faculty of Science, Utrecht University, 3584 CH Utrecht, The Netherlands

Received October 15, 2012, and in revised form, January 9, 2013
Published, MCP Papers in Press, February 11, 2013, DOI 10.1074/mcp.M112.024950

[1] The abbreviations used are: Ercc1, excision repair cross-complementing group 1; KO, knock-out; SAM, significance analysis of microarrays; SCX, strong cation exchange; IHC, immunohistochemistry.

from other organs (*i.e.* liver and kidney) or general tissue stress responses. Therefore, the changes observed in animal behavior and protein expression levels can be attributed to the specific cell type that is affected, and the surroundings in which it directly interacts. Purkinje cells are neurons that act as signal converters in the cerebellar cortex and are essential for the proper functioning of the cerebellum. Their main role is to convert input signals from many different neurons into the sole output signal of the cerebellum, thereby controlling motor coordination, learning, and cognitive functions.

Until now, most neuroproteomics studies have been directed at general protein composition of the synapse, with the emphasis on the synaptosomes (9), synaptic membranes (10, 11), or post- and pre-synaptic densities (8, 12) by using subcellular fractionation strategies on the whole brain or subcompartments. Here, we compared quantitatively the proteome from intact cerebella from Purkinje neuron-specific DNA-repair KO mice with cerebella from control mice at the age of 8, 16, and 26 weeks to monitor aging-related molecular changes in the cerebellum over time. Using this mouse model coupled with stable isotope dimethyl labeling and high resolution nanLC-MS, we were able to quantify the proteins present in *ex vivo* cerebellum Purkinje synapses without introducing any bias induced by subcellular fractionation methods or artificial cell culture systems. A small set of consistently down-regulated proteins originated from a strongly interconnected network known to be involved in synaptic signaling. Furthermore, immunohistochemistry experiments were performed to confirm mass spectrometry data and to assess protein localization as well as Purkinje cell and cerebellum morphology.

EXPERIMENTAL PROCEDURES

Mouse Models—The generation and characterization of *Ercc1*$^{+/-}$ mice has been described previously (5). To achieve Purkinje cell-specific *Ercc1* gene inactivation, a transgenic line with Cre recombinase under the control of the L7/pcp2 promoter was used (13). Female *L7/pcp2-Cre*$^{+}$ mice were crossed with male *Ercc1*$^{+/-}$ mice (both in the C57BL6J background). Female *Ercc1*$^{+/-}$ *L7/pcp2-Cre*$^{+}$ mice, obtained from these breedings, were crossed with male *Ercc1*$^{f/f}$ FVB mice to yield hybrid *Ercc1*$^{f/-}$ *L7/pcp2-Cre*$^{+}$ mice. The homozygous *Ercc1*$^{f/f}$ mice (floxed Ercc1; with loxP sites inserted into its *Ercc1* gene) (14) were kindly provided by Dr. D. W. Melton (University of Edinburgh, Edinburgh, Scotland, UK) and backcrossed for 10 generations to obtain a pure FVB background. *Ercc1*$^{f/-}$ *L7/pcp2-Cre*$^{+}$ mice (in the F1 C57BL6J/FVB hybrid background) are heterozygous for *Ercc1* in their entire body, except for the Purkinje cells in the cerebellum, which are homozygous for *Ercc1* after Cre excision of the floxed allele. These mice will be referred to as KO in the remainder of the study. As controls, we used *Ercc1*$^{f/+}$ *L7/pcp2-Cre*$^{+}$ littermates (referred to as control), which are wild type in their entire body, except for the Purkinje cells in the cerebellum, which are heterozygous.

All animals used in the studies described in this paper were of the same F1 C57BL6J/FVB hybrid background and had *ad libitum* access to standard mouse food (CRM pellets, SDS BP Nutrition Ltd.; gross energy content 18.36 kJ/g dry mass, digestible energy 13.4 kJ/g) and water. Mice were weighed, visually inspected weekly, and scored for gross morphological and motor abnormalities. Experiments were performed in accordance with the Principles of Laboratory Animal Care (National Institutes of Health publication no. 86-23) and with the guidelines approved by the Erasmus University Animal Care Committee.

Sample Preparation—Frozen female cerebella were lysed by sonication in lysis buffer (8 M urea in 50 mM ammonium bicarbonate, 1 tablet of Complete mini EDTA-free mixture (Roche Applied Science), and 1 tablet of PhosSTOP phosphatase inhibitor mixture (Roche Applied Science)). After centrifugation (20,000 × *g* 30 min at 4°C), the supernatant was assayed for protein content using the BCA kit standard procedure (Pierce) (~4 mg per condition). Protein reduction and alkylation were performed using final concentrations of 2 mM dithiothreitol and 4 mM iodoacetamide, respectively. A first enzymatic digestion step was performed in 8 M urea lysis buffer using Lys-C at 37 °C for 4 h (enzyme/substrate ratio 1:75). The second digestion was performed overnight (37 °C) with trypsin (enzyme/substrate ratio 1:100) in 2 M urea. Resulting peptides were chemically labeled using stable isotope dimethyl labeling as described before (15). In the first experiment, control tissue was labeled "Intermediate," and *Ercc1* PkJ KO was labeled "Heavy. " In the second replicate experiment, the Intermediate (I) and Heavy (H) labels were swapped. In both experiments, a 1:1:1 mixture of control tissue lysates of 8, 16, and 26 weeks was labeled "Light" (L) as an internal control. The labeling efficiency for all labels was higher than 96%. Next, an aliquot of each label was measured on a regular LC-MS/MS run, and samples were mixed 1:1:1 (L/I/H) based on their peptide intensities. This was found to result in a more precise ratio than using the total protein amounts as determined by a BCA assay. After mixing, peptides were dried to completion and subsequently reconstituted in 10% formic acid prior to fractionation using strong cation exchange (SCX) as described previously (16). Briefly, SCX was performed using a Zorbax BioSCX-Series II column (0.8-mm inner diameter × 50-mm length, 3.5 μm). SCX solvent A consisted of 0.05% formic acid in 20% acetonitrile and solvent B of 0.05% formic acid, 0.5 M NaCl in 20% acetonitrile. The SCX gradient was as follows: 0–0.01 min (0–2% B); 0.01–8.01 min (2–3% B); 8.01–14.01 min (3–8% B); 14.01–28 min (8–20% B); 28–38 min (20–40% B); 38–48 min (40–90% B); 48–54 min (90% B); and 54–60 min (0% B). After injection of 200 μg of labeled tissue lysate, a total of 45 SCX fractions was collected per cell lysate and dried in a vacuum centrifuge.

Liquid Chromatography and Mass Spectrometry—After reconstituting the SCX fractions containing doubly and triply charged peptides (~15 fractions in each SCX) in 10% formic acid, peptides were analyzed using nano-flow reverse phase liquid chromatography coupled to a LTQ-Orbitrap Velos mass spectrometer (Thermo, San Jose, CA). Depending on the SCX UV trace, 1–10% of each fraction was injected. Densely populated 2+ fractions were injected twice to minimize under-sampling of the mass spectrometer. Peptides were trapped on a trap column (ReproSil-Pur C18-AQ, 3 μm (Dr. Maisch GmbH, Ammerbuch, Germany); 20 mm × 100 μm inner diameter, packed in house) at 5 μl/min in 100% solvent A (0.1 M acetic acid in water). Next, peptides were eluted from the trap column onto the analytical column (ReproSil-Pur C18-AQ, 3 μm (Dr. Maisch GmbH, Ammerbuch, Germany); 40 cm × 50-μm inner diameter, packed in house) at ~100 nl/min in 1-, 2-, or 3-h gradients from 10 to 50% solvent B (0.1 M acetic acid in 8:2 (v/v) acetonitrile/water). Nanospray was achieved with an in-house pulled and gold-coated fused silica capillary (360 μm outer diameter; 20 μm inner diameter; 10 μm tip inner diameter) and an applied voltage of 1.7 kV. The mass spectrometer was configured to perform a Fourier transform survey scan from 350 to 1,500 *m/z* (resolution 30,000) followed by higher collision energy dissociation fragmentation of the 10 most intense peaks (35% normalized collision energy at a target value of 50,000 ions, resolution 7,500).

Data Analysis—All MS data were processed with Proteome Discover (version 1.3, Thermo Scientific, Bremen, Germany) using a standardized workflow. Peak lists, generated in Proteome Discover, were searched against a concatenated forward-decoy Swiss-Prot (version 56.2, taxonomy *Mus musculus,* 32 402 protein entries) database, supplemented with frequently observed contaminants, using Mascot (version 2.3.02 Matrix Science, London UK). The following search parameters were used: 50 ppm precursor mass tolerance, 0.05-Da fragment ion tolerance, trypsin cleavage with maximum of two miscleavages, cysteine carbamidomethyl static modification and methionine oxidation, and dimethyl labeling (L, I, and H) of lysine residues and the peptide N termini as dynamic modification. Triplex dimethyl labeling was used as a quantification method, with a mass precision of 2 ppm for consecutive precursor mass scans and a normalization on the mean peptide ratio. An RT tolerance of 0.5 min was used to account for the effect of deuterium on the retention time. To filter for high quality data and to control the false discovery rate on identifications, only the peptide spectral matches adhering to the following criteria were kept for analysis: minimal Mascot score of 20, minimal peptide length of 7, only unique rank 1 peptide, and a mass deviance of 20 and 10 ppm for experiment 1 and experiment 2, respectively. As a result, we obtained a peptide false discovery rate of 0.89% for experiment 1 and 0.79% for experiment 2. To distinguish between proteins with high similarities, only unique peptides were considered for protein identification and quantification. The estimation of the false discovery rate in quantification was calculated using significance analysis of microarrays (SAM), which is increasingly used by the proteomics community because conventional *t* testing tends to result in an underestimation of false-positives (17–19). The obtained SAM *q* value is the empirically estimated false discovery rate per individual protein and should therefore not be interpreted as a global false discovery rate or *p* value. The *q* values were obtained using the multiexperiment viewer (MeV version 4.6.2) with the method proposed by Tusher *et al.* (20) using 1,000 permutations. Proteins with a minimum rounded average 2.0-fold change and a *q* value below 0.1 were considered significantly regulated.

Antibodies—Primary antibodies used in this study were as follows: rabbit anti-Calbindin (Calb1) (Swant; 1:10,000); rabbit anti-cleaved caspase-3 (CASP-3) (Asp-175; Cell Signaling Technology; 1:500); rabbit anti-connexin43 (CX43) (Abcam; 1:1,000); rabbit anti-GFAP (DAKO; 1:8,000); rabbit anti-GluRδ1/2 (Chemicon; 1:1,000); rabbit anti-HtrA1 (Abcam; 1:100); rabbit anti-Itpr1 (Abcam; 1:2,500); rat anti-Mac2 (Cedarlane; 1:1,000); rabbit anti-PKCγ (Santa Cruz Biotechnology; 1:2,000); and goat anti-Prkg1 (cGK1) (Santa Cruz Biotechnology; 1:500). For avidin-biotin-peroxidase immunocytochemistry, biotinylated secondary antibodies (Vector Laboratories; 1:200) were used.

Immunohistochemical Procedures—Mice were anesthetized with pentobarbital and perfused transcardially with 4% paraformaldehyde. The brain was carefully dissected out and postfixed overnight in 4% paraformaldehyde. Routinely, brain tissue was embedded in 10% gelatin blocks, rapidly frozen, and sectioned at 40 μm with a freezing microtome or stored at −80 °C until use (21). Control and KO tissue was embedded together, in one gelatin block per time point, to avoid fluctuations in antibody affinity. To quantitatively assess protein regulation using IHC results, all immunohistochemical procedures were performed simultaneously for each antibody. Sections were processed, free-floating, using a standard avidin-biotin-immunoperoxidase complex method (ABC, Vector Laboratories, Burlingame, CA) with diaminobenzidine (0.05%; Sigma-Aldrich) as the chromogen as described previously (21). In addition, a selected number of frozen gelatin sections was collected in 4% paraformaldehyde and processed with the modified Gallyas silver impregnation procedure of Nadler and Evenson (22) that selectively labels degenerating neurons and their processes. Immunoperoxidase-stained sections were analyzed and photographed using an Olympus BX40 microscope and a ColorView digital camera. Quantification was performed using MetaMorph Image Analysis software (Molecular Devices, Sunnyvale, CA). Background intensity was subtracted per antibody, and the average intensity of the 8-week control sample was set to 1. Statistical significance was calculated by analysis of variance with a Bonferroni post-test to compare the replicate means by age using Prism (GraphPad Software, Inc., La Jolla, CA).

RESULTS

To decipher the molecular changes that underlie the observed phenotype, an in-depth quantitative proteomics screen was performed with biological duplicates (and technical duplicates) on cerebella from control and Purkinje cell-specific *Ercc1*$^{f/-}$ knock-out mice. The knock-out mice have the same life span as compared with wild type littermates and show normal growth development. At the age of 8 weeks, the Purkinje-specific *Ercc1* KO mice showed no aberrant behavior and were phenotypically undistinguishable from littermate controls. Around 16 weeks the normal weight gain of these animals starts to level off (Fig. 1*A*). Furthermore, the first signs of imbalance were observed at this stage and developed into severe motoric dysfunctioning at 26 weeks. The observed motor abnormalities are similar to the *Ercc1*$^{\Delta/-}$ full body mutant mice (23) and were not present in any of the control animals. Comprehensive behavioral studies of the Purkinje-specific *Ercc1* KO mice further showed a clear motoric function decline and lack of capacity in motoric learning at 26 weeks.[2] Based on the phenotypical behavior, three time points for tissue analysis were chosen as follows: an early time point at 8 weeks to search for molecular markers before the onset of the observed phenotype; an intermediate time point at 16 weeks; and a late time point at 26 weeks, where major molecular changes are anticipated.

After dissection of the cerebella, the tissue was processed as described in the workflow in Fig. 1*B*. To compare protein levels from control and KO mice, the generated peptides were labeled with medium and heavy dimethyl stable isotope labels, respectively (15). As an internal control, a mixture of all control samples was labeled with a light version of dimethyl. Next, the internal control sample was mixed with equal protein amounts of control and KO samples per time point (1:1:1 ratio). To decrease sample complexity, per time point, each peptide mixture was fractionated using SCX in which the 14 main fractions were analyzed by reverse phase LC-MS using an Orbitrap Velos with higher collision energy dissociation fragmentation. Peptide identities and ratios between control (medium) and KO (heavy) were analyzed using Proteome Discoverer software, Bremen, Germany. In the biological replicate experiment, the same procedure was followed, with the exception of a stable isotope label-swap between control and KO samples. In total, 5,254 proteins could be identified and quantified from all cerebella, over all time points (supplemental Tables S1 and S2).

[2] van der Vaart, T., Elgersma, Y. manuscript in preparation.

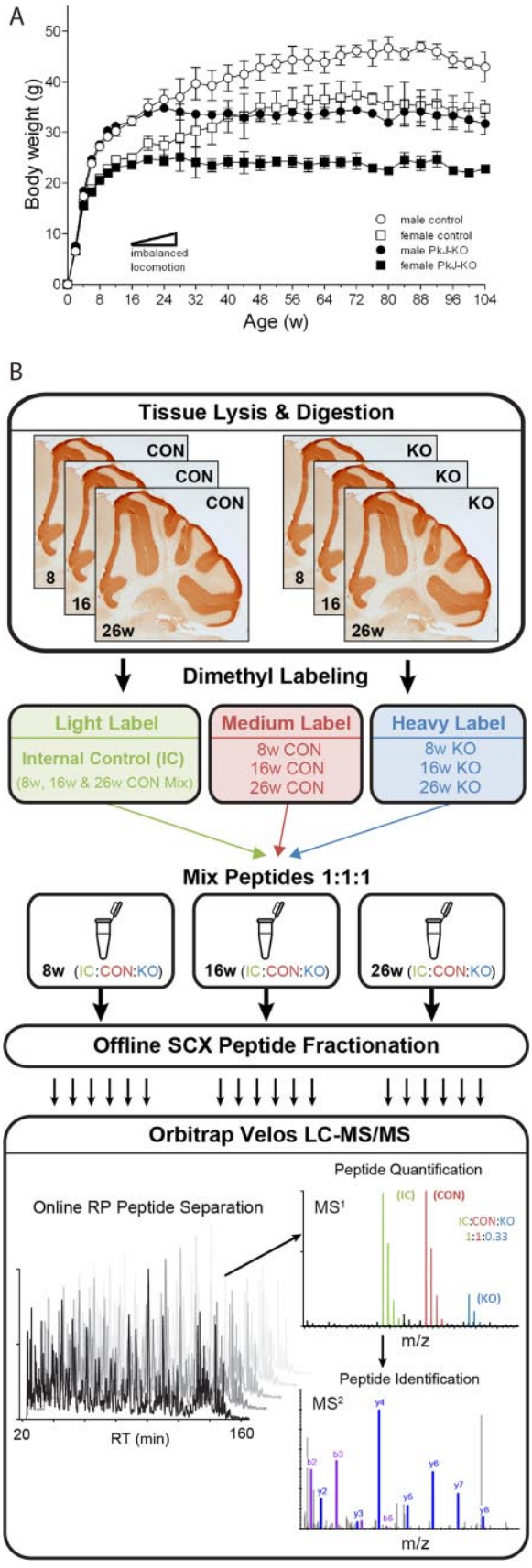

To compare protein expression levels between control and KO replicates, their logarithmic ratios were plotted against each other (Fig. 2). Proteins with an average regulation from both replicates of at least 2-fold up or down, and a SAM *q* value below 0.1, are considered to show a significant expression change. When comparing the KO/control ratios of two replicates, the left top and right bottom quadrant show the proteins that are consistently regulated in both replicates. Proteins located in the remaining two quadrants show an anticorrelation between both replicates and were found to be originating from contaminants and low confidence, single peptide quantifications.

Ex Vivo Proteomic Screenings of Progeroid Cerebella—At 8 weeks of age (postnatal day (P) 56), the cerebella of control and KO mice are similar in morphology (supplemental Fig. S1, *A* and *B*). When looking at the protein levels, a similar trend was observed. The log ratio between *Ercc1* Purkinje KO and control are close to zero for both replicates, as can be seen by the circular distribution of the replicate ratios (Fig. 2*A*). The proteins that are consistently regulated in both replicates (Clic6, E-NPP2, and Lat2) were not significantly changed in the later time points and did not show any functional relationship; therefore, these proteins were discarded from further analysis.

At 16 weeks (P112), the sizes of KO cerebella were still comparable with control; however, the individual protein ratios were already starting to show significant changes between control and KO tissue. Although most of the protein levels remained unchanged, the data distribution is starting to stretch out from the circular distribution into the two quadrants representing protein regulation (Fig. 2*B*). This trend is not observed when comparing the protein expression of control tissue of 8 and 16 weeks with 26-week-old control cerebella, proving the observed trend in KO is caused solely by the silencing of the *Ercc1* gene and not for temporal/developmental reasons (supplemental Fig. S2, *A* and *B*). Among the consistently regulated proteins at 16 weeks, 27 proteins were found to be up- or down-regulated. The identity of the regulated proteins revealed a down-regulation of proteins involved in synaptic signaling (GluRδ2, Delphilin, and IP3R1) and signal transduction (cGK1, PKCγ, Ahrgef33, RGS8, TN-C, and Ppp1r16b). Furthermore, the increase in astrocyte marker GFAP and complement factor C1qb indicates neuronal damage and an inflammatory response.

FIG. 1. *A,* phenotypical weight and motoric function data of Purkinje cell-specific *Ercc1* KO mice. *B,* proteomics workflow scheme. After cerebellum dissection from mice of different genetic background and age, tissues were lysed in 8 M urea and digested with Lys-C and trypsin. Internal control, control, and knock-out peptides were labeled using stable isotope dimethyl labeling and mixed in three groups corresponding to the age of the sacrificed mice. In the replicate experiment, heavy and medium labels were swapped. Sample complexity was reduced by generating 14 SCX fractions from each time point prior to a 3-h LC-MS/MS analysis on an Orbitrap Velos.

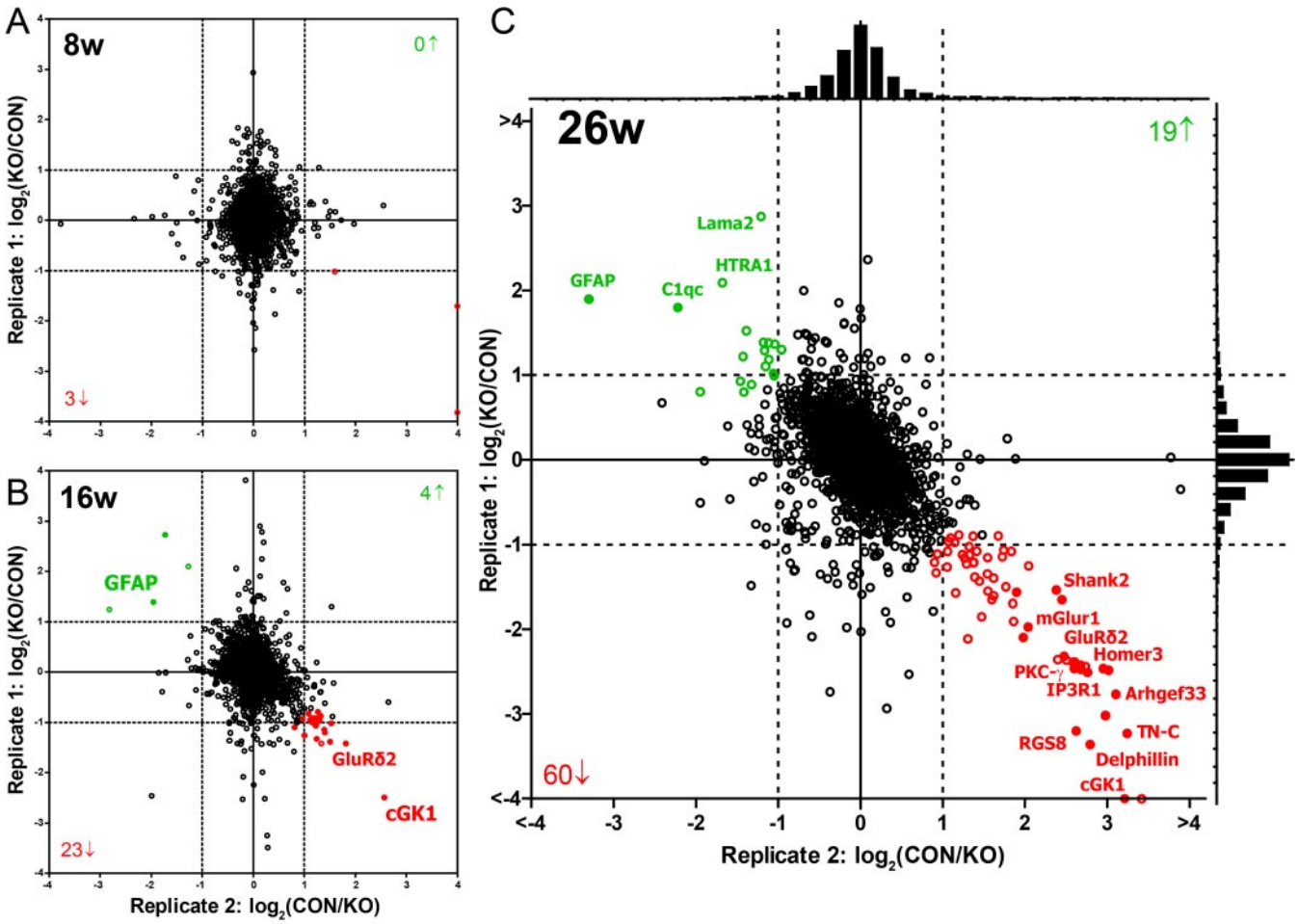

FIG. 2. **Knock-out *versus* control protein ratio plotted for replicate 1 *versus* replicate 2.** Logarithmic protein ratios were plotted for 8-week-old (*8w*) (*A*), 16-week-old (*16w*) (*B*), and 26-week-old (*26w*) (*C*) mice. Over 3,000 proteins were quantified per time point. Proteins regulated after both 16 and 26 weeks are indicated by *closed colored circles*. Proteins with an average 2-fold regulation and a SAM *q* value below 0.1 were considered significant.

After 26 weeks (P182), a specific reduction in cerebella size is observed in KO mice as compared with control brains, whereas all other parts of the brain were unaffected (supplemental Fig. S1, *C* and *D*). Using the dimethyl labeling strategy, equal amounts of proteins are compared, taking into account the variation of cerebellum size. This resulted in ~98% of all proteins showing <2-fold expression changes, albeit with a clear difference in overall distribution of protein levels between control and knock-out tissue (Fig. 2*C*). Although such a small number of changes in protein expression (approximately <2%) is in line with a study by Walther and Mann (24) in which no extensive proteome changes were observed in the cerebella of healthy 5- and 26-month-old mice, it shows a remarkable robustness in protein expression levels as our progeroid model displays aberrant neurological behavior and visible brain morphological changes at 26 weeks. Interestingly, the proteins found to be down-regulated after 16 weeks were further down-regulated after 26 weeks, indicating a reproducible and predictable model system (Fig. 2*C*). In addition to the proteins regulated after 16 weeks, a new set of regulated proteins emerged in the KO cerebella after 26 weeks. In total, 60 proteins were down-regulated and 19 proteins were found to be up-regulated using our strict criteria.

Molecular Function of Regulated Proteins—The proteins found to be up-regulated in KO tissues contained the astrocyte marker GFAP, a gap junction glial marker protein connexin43 (Cx43), macrophage marker Mac-2, complement factor C1qC, as well as metallothionein 1 (Mt-1). The up-regulation of these classes of proteins marks an increased recruitment of astrocytes and/or other glial cells indicating an increase in neuronal damage and inflammation in the cerebellum of KO mice. This is in line with previous studies that have shown that aging and the lack of efficient DNA repair can trigger neurodegenerative and inflammatory processes (23, 25–27). Other proteins found to be up-regulated are extracellular proteins that are known to interact with or modify the extracellular environment (HTRA1 and Lama2) as well as cell adhesion molecules (PECAM-1 and MCAM). Caspase-3 was

TABLE I
Proteins differentially expressed in mouse cerebellum upon Purkinje cell DNA damage

UniprotKB accession no.	Protein name	Description	8w FC[a]	16w FC[a]	26w FC[a]	*q* value
Classical Purkinje cell markers						
P12658	Spot 35/Calbindin	Calbindin	−0.1	−0.9	−2.4	0.000
P12660	L7/Pcp2	Purkinje cell protein 2	−0.1	−1.1	−2.6	0.000
P63054	PEP-19/Pcp4	Purkinje cell protein 4	0.0	−0.8	−1.6	0.000
Transmembrane proteins						
P97772	mGluR1	Metabotropic glutamate receptor 1	−0.1	−1.0	−2.0	0.000
Q61625	GluRδ2	Glutamate receptor δ-2 subunit	−0.2	−1.5	−2.4	0.000
P23818	GluR-1	Glutamate receptor 1, AMPA1	0.3	−0.4	−1.1	0.027
Q9WV18	GABABR1	γ-Aminobutyric acid type B receptor subunit 1	−0.1	−0.6	−1.4	0.027
Q80T41	GABABR2	γ-Aminobutyric acid type B receptor subunit 2	−0.1	−0.8	−1.3	0.017
P11881	IP3R1	Inositol 1,4,5-trisphosphate receptor type 1	−0.1	−1.1	−2.6	0.000
Q9Z329	IP3R2	Inositol 1,4,5-trisphosphate receptor type 2	0.0	−0.9	−2.6	0.000
O55143	SERCA2	Sarcoplasmic/endoplasmic reticulum calcium ATPase 2	0.0	−0.5	−1.0	0.016
Q64518	SERCA3	Sarcoplasmic/endoplasmic reticulum calcium ATPase 3	−0.1	−1.0	−2.8	0.000
Q9QZC1	TrpC3	Short transient receptor potential channel 3	0.1	−0.9	−4.5	0.019
P63143	$K_v\beta1$	Voltage-gated potassium channel subunit β-1	−0.1	−0.7	−1.2	0.016
Q6PHS9	$Ca_v\alpha2\delta2$	Voltage-gated calcium channel subunit δ-2	−0.3	−0.8	−1.2	0.017
O35544	Eaat4	Excitatory amino acid transporter 4	−0.2	−0.9	−1.9	0.000
Q5DTL9	Slc4a10	Sodium-driven chloride bicarbonate exchanger	−0.2	−0.6	−1.2	0.050
Q921R8	Slc41a3	Solute carrier family 41 member 3	0.2	−0.9	−1.4	0.084
Q6WQJ1	DGL-α	S_n1-specific diacylglycerol lipase α	−0.1	−1.1	−2.5	ND*
Q8JZM4	DNER	δ and Notch-like epidermal growth factor-related receptor	−0.2	−0.9	−1.5	0.000
Q8C5W0	Calmin	Calmin/Calponin-like transmembrane domain protein	0.0	−1.0	−1.7	0.000
Q6NXK7	DPP X	Dipeptidyl peptidase X	−0.1	−0.6	−1.5	0.000
Q62092	Nsg1	Neuron-specific protein family member 1	−0.3	−0.5	−1.2	0.017
Q3UH99	Shisa6	UPF0626 protein B	−0.2	−1.0	−1.1	0.081
Q8K0T0	Rtn1	Reticulon-1	0.0	−0.5	−1.0	0.061
P41731	Cd63	CD63 antigen	0.1	0.4	1.1	0.082
P41233	ABC-1	ATP-binding cassette subfamily A member 1	ND*	0.5	1.2	0.082
Q08481	PECAM-1	Platelet endothelial cell adhesion molecule (CD31)	ND*	ND*	1.1	0.082
Q8R2Y2	MCAM	Cell surface glycoprotein MUC18/melanoma cell adhesion molecule/CD146	0.4	0.8	1.4	0.082
P23242	Cx43	Gap junction α-1 protein/Connexin-43	0.4	0.5	1.3	0.082
Extracellular proteins						
Q80YX1	TN-C	Tenascin-C/Hexabrachion	0.0	−1.6	−3.2	0.000
P02802	MT-1	Metallothionein-1	−0.1	0.5	1.1	0.082
P03995	GFAP	Glial fibrillary acidic protein	0.0	1.7	2.6	0.082
Q9R118	HTRA1	Serine protease HTRA1	−0.1	0.3	1.9	0.082
Q60675	Lama2	Laminin subunit α-2/laminin M	0.7	0.6	2.0	0.082
Scaffold proteins						
Q0QWG9	Delphilin	Delphilin/Glutamate receptor, ionotropic, δ2-interacting protein 1	−0.1	−1.3	−3.1	0.000
Q6WVG3	Kctd12	BTB/POZ domain-containing protein KCTD12	0.0	−0.6	−1.1	0.017
Q80Z38	Shank2	SH3 and multiple ankyrin repeat domains protein 2	0.0	−1.1	−2.0	0.029
Q99JP6	Homer-3	Homer protein homolog 3	−0.1	−1.1	−2.5	0.000
O54931	Akap2	A-kinase anchor protein 2	−0.2	−0.7	−1.4	0.000

TABLE I—*continued*

UniprotKB accession no.	Protein name	Description	8w FC[a]	16w FC[a]	26w FC[a]	*q* value
Signaling proteins						
P11798	CaMK-IIα	Calcium/calmodulin-dependent protein kinase type II α chain	0.0	−0.9	−1.7	0.071
P63318	PKCγ	Protein kinase C γ type	−0.1	−1.3	−2.5	0.000
P0C605	cGK1	cGMP-dependent protein kinase 1, α isozyme	−0.4	−2.5	−3.3	ND*
Q8CG03	Pde5a	cGMP-specific 3′,5′-cyclic phosphodiesterase	−0.4	−1.0	−2.7	0.000
Q8R071	IP3KA	Inositol-trisphosphate 3-kinase A	0.0	−1.1	−3.0	0.000
Q9EPW0	Inpp4a	Type I inositol-3,4-bisphosphate 4-phosphatase	0.0	−0.6	−1.3	0.026
Q91WG7	DGK-γ	Diacylglycerol kinase γ	0.0	−0.6	−1.0	2.957
Q80UP3	DGK-ζ	Diacylglycerol kinase ζ	0.1	−0.9	−1.7	0.079
Q8BW86	Arhgef33	Rho guanine nucleotide exchange factor 33	0.0	−1.3	−2.9	0.000
Q8BXT1	RGS8	Regulator of G-protein signaling 8	−0.1	−1.3	−2.9	0.000
Q9JMF3	GNG13	Guanine nucleotide-binding protein G(I)/G(S)/G(O) subunit γ-13	−0.1	−1.1	−2.1	0.016
P57759	Erp29	Endoplasmic reticulum protein ERp29	0.0	−0.6	−1.4	0.000
P68510	14-3-3η/Ywhah	14-3-3 protein η	−0.1	−0.4	−1.0	0.050
Cytosekeletal proteins						
Q9JJZ2	Tuba8	Tubulin α-8 chain	−0.2	−0.8	−1.8	0.000
P97434	RIP3	Myosin phosphatase Rho-interacting protein	−0.3	−0.7	−1.6	0.000
Q05BC3	EMAP-1	Echinoderm microtubule-associated protein-like 1	0.0	−0.4	−1.3	0.000
Q3UJU9	RMD-3	Regulator of microtubule dynamics protein 3	0.1	−0.6	−1.6	0.000
Q8R1S4	Mtss1	Metastasis suppressor protein 1	−0.1	−0.9	−2.4	0.000
Cytosolic and remaining proteins						
P28651	CARP	Carbonic anhydrase-related protein	−0.1	−1.1	−2.6	0.000
Q3TGF2	Fam107b	Protein FAM107B	−0.1	−1.1	−2.0	0.000
Q99K30	EPS8-LP2	Epidermal growth factor receptor kinase substrate 8-like protein 2	−0.1	−1.1	−2.5	0.000
Q9ERG2	Striatin-3	Striatin-3/Cell cycle autoantigen SG2NA	0.2	−0.7	−1.6	0.000
P62748	Hpcal1	Hippocalcin-like protein 1/Neural visinin-like protein 3	0.0	−0.7	−1.3	0.017
Q61704	ITI-HC3	Inter-α-trypsin inhibitor heavy chain H3	0.1	−0.6	−1.7	0.020
Q9ERQ8	CA-VII	Carbonic anhydrase 7	0.2	−0.8	−1.4	0.028
Q8BKX1	BAI-ap2	Brain-specific angiogenesis inhibitor 1-associated protein 2/Insulin receptor substrate p53	−0.1	−0.8	−1.2	0.030
Q1RLL3	Copine-9	Copine-9	−0.1	−0.7	−1.4	0.081
Q9CRD4	Dbndd2	Dysbindin domain-containing protein 2	0.2	−0.9	−1.5	0.082
Q80ZW2	Them6	UPF0670 protein THEM6 homolog	0.0	0.0	−1.1	0.084
Q3UVC0	Ksr2	Kinase suppressor of Ras 2	−0.4	−0.9	−1.1	0.086
Q8BIZ1	AIDA-1	Amyloid-β protein intracellular domain-associated protein 1	0.0	−0.7	−1.3	0.097
P28828	R-PTPμ	Receptor-type tyrosine-protein phosphatase mu	0.2	−0.2	−1.1	0.078
Q02105	C1qc	Complement C1q subcomponent subunit C	ND*	ND*	2.0	0.082
P20152	Vim	Vimentin	0.1	0.2	1.1	0.082
P20060	Hexb	β-Hexosaminidase subunit β	0.4	0.7	1.2	0.082
O70370	Ctss	Cathepsin S	0.3	0.8	1.2	0.082
Q06890	Clu /ApoJ	Clusterin/Apolipoprotein J	0.0	1.0	1.4	0.082
Q8BVW0	Ganc	Neutral α-glucosidase C	−0.2	0.1	1.0	0.082
Q08642	Padi2	Protein-arginine deiminase type-2	0.0	0.8	1.3	0.082
Q8VDD9	PHIP	PH-interacting protein/Neuronal differentiation-related protein	0.0	−0.7	1.0	0.082
Q8BVW0	Ganc	Neutral α-glucosidase C	−0.2	0.1	1.0	0.082
Q9R0M4	PCLP-1	Podocalyxin-like protein 1	−1.2	0.3	1.2	0.082
Q8VHQ3	Ppp1r16b	Protein phosphatase 1 regulatory inhibitor subunit 16B	−0.1	−1.4	ND*	ND*

TABLE I—*continued*

UniprotKB accession no.	Protein name	Description	8w FC[a]	16w FC[a]	26w FC[a]	*q* value
P16110	Gal-3/Mac-2	Galectin-3, Mac-2 antigen	ND*	1.6	3.0	0.081
P23927	Cryab	α-Crystallin B chain	−0.1	0.4	1.1	0.082
P42574	CASP-3	Caspase 3	0.6	ND	3.8	ND*

[a] FC indicates log2 fold change of protein expression between control and KO cerebella after 8 weeks (8w), 16 weeks (16w), and 26 weeks (26w) of age. * means not quantified in one or two replicates due to absence in KO or control tissue (possibly an on/off-regulation). *q* values were calculated for protein ratios from 26-week-old mice.

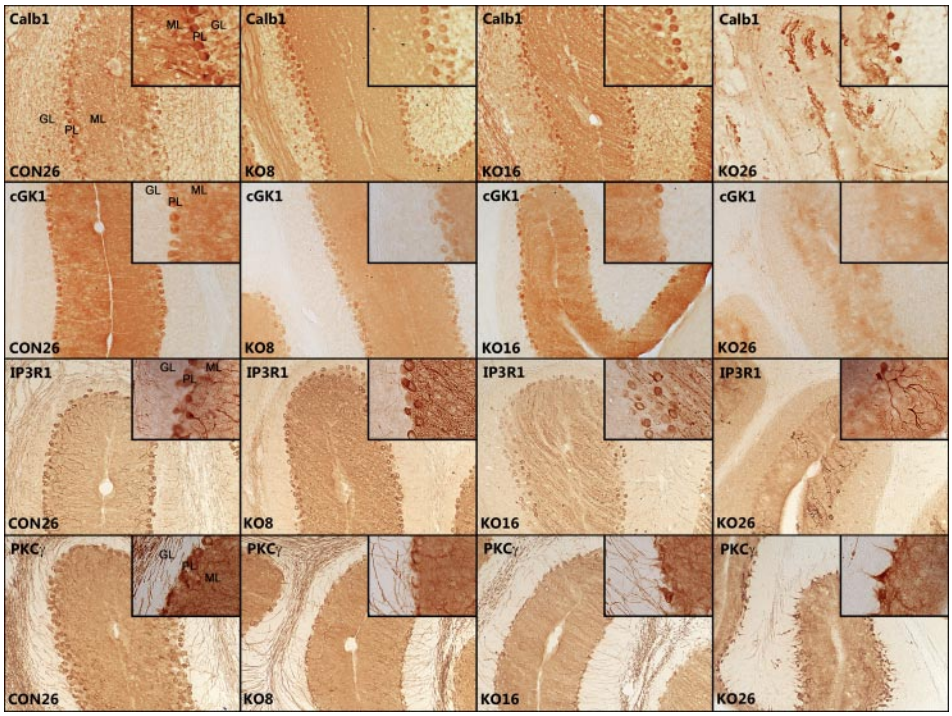

FIG. 3. **Immunohistochemical staining of regulated proteins reveals a decrease in synaptic proteins of DNA-repair compromised Purkinje cells.** Calbindin (*Calb1*), cGMP-dependent protein kinase 1 (*cGK1*), inositol 1,4,5-trisphosphate receptor type 1 (*IP3R1*), and PKCγ were found to be present only in Purkinje cells. When comparing 26-week-old control (*CON26*) with 8-, 16-, and 26-week-old knock-out mice (*KO8*, *KO16*, and *KO26*, respectively), an overall decrease of all four proteins is observed in *Ercc1* KO mice over time. The organization of down-regulation is different among the proteins. cGK1 is completely removed after 26 weeks, whereas Calbindin and IP3R1 are still present in a few Purkinje cells. PKCγ is still present in most Purkinje cell bodies after 26 weeks, indicating the enormous morphological changes that Purkinje neurons undergo upon DNA damage. Photographs were taken using ×100 and ×400 (*insets*) magnifications.

also found to be up-regulated; however, the ratio between KO and control experiment could not be calculated in one replicate due to low protein levels in control tissue. The increase of caspase enzymes could indicate an elevated level of apoptotic cells, due to excessive DNA damage or locally activated apoptotic synaptic cascades influencing synaptic plasticity (28).

The group of down-regulated proteins contained synaptic scaffold proteins (*i.e.* Homer-3 and Shank2), neurotransmitter receptors (*i.e.* mGluR1, GluRδ2, GABABR1, and GABABR2), ion channels/transporters (*i.e.* SERCA3, TrpC3, $K_v\beta1$, and $Ca_v\alpha2\delta2$), and signal transduction enzymes (*i.e.* cGK1, PKC-γ, CaMK-IIα, IP3KA, and Pde5a). Many of these proteins are known to be present in synapses of different types of neurons throughout the brain indicating a strong effect of DNA damage on synaptic maintenance. Interestingly, it has been described that reduced synaptic contact and activity are some of the early hallmarks of neurodegenerative diseases (26, 29). Therefore, the down-regulated proteins found in this study can be considered as a set of proteins that are specifically expressed and active in Purkinje pre- and post-synaptic areas and potentially define the Purkinje synapses. A complete list of all regulated proteins, including Purkinje cell markers L7 (Purkinje cell protein 2), Spot 35 (Calbindin), and PEP-19 (Purkinje cell protein 4), and their SAM *q* value, can be found in Table I.

In addition to proteins with known signaling transduction routes also signaling molecules without known interaction partners like Arhgef33, RGS8, and GNG13 were found to be regulated. These proteins were predicted to be involved in

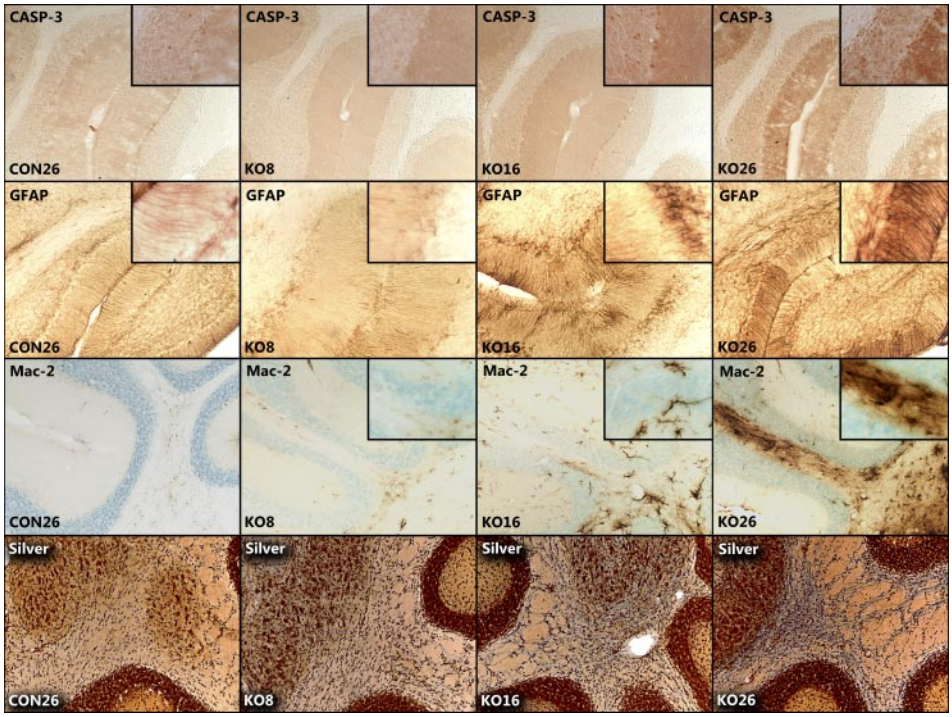

FIG. 4. **Immunohistochemical staining of regulated proteins reveals protein regulation in different layers of mice cerebella.** A strong increase in activated Caspase 3 (*CASP-3*) and the astrocyte marker (*GFAP*) is observed in the molecular layer of Purkinje KO mice cerebella over time (*KO8*, *KO16*, and *KO26*, respectively), indicating dendritic reorganization. The probing of activated macrophages (*Mac-2*) and staining of neurodegenerative tissue by a silver staining (*Silver*) indicate neuronal damage is primarily located to the white matter layer of mice bearing a defective DNA-repair mechanism in their Purkinje cells. Photographs were taken using ×100 and ×400 (*insets*) magnifications.

G-protein-coupled signaling based on their homology to known protein domains. However, their exact function and interaction partners are not known. In the proteomics data, these proteins are strongly co-regulated with other synaptic proteins, suggesting a functional role in the Purkinje synaptic signal transduction cascades. A possible role for these proteins could involve binding to similarly regulated G-protein-coupled receptors (*i.e.* mGluR1) and their scaffold proteins (*i.e.* Homer-3), thereby activating other ion channels (*i.e.* IP3R1 and -2 and TrpC3) or signal transduction cascades (*i.e.* cGK1 and CaMK-IIa) that are part of the same scaffold complex or in the nearby vicinity.

Immunohistochemistry Validation and Follow-up—To verify our proteomics results, a set of proteins was analyzed by IHC staining in sagittal sections of mouse brains from the three different time points. The great advantage over commonly used verification methods by Western blot is the ability to localize protein changes in different substructures of the cerebellum. An additional benefit is that cell type specificity and even subcellular (*i.e.* axon, cell body, or dendrite) regulations can be observed. The spatial semi-quantitative IHC data of the validated proteins is plotted in supplemental Fig. S4, corroborating our proteomics based protein quantification.

The protein Calbindin is commonly used as a marker for Purkinje cells and was therefore used as a positive control for our immunohistochemistry procedures. It should be clear that Calbindin is indeed only present in the Purkinje cell body, axon, and dendrites residing in the Purkinje, granular, and molecular layer, respectively (Fig. 3). For the DNA-repair knock-out mice, both the proteomics data and immunohistochemistry data showed a strong reduction in Calbindin levels and number of Calbindin-positive cells over time (Fig. 3 and supplemental Fig. S3). Furthermore, the staining for the inositol 1,4,5-trisphosphate-activated calcium channel type 1 (IP3R1), cGMP-dependent protein kinase 1 (cGK1), protein kinase Cγ type (PKCγ), and glutamate receptor δ-2 subunit (GluRδ2) confirmed the strong abundance and down-regulation in Purkinje cells observed by the proteomics screening (Fig. 3 and supplemental Figs. S3, S4, and S5*A*). Although Calbindin and PKCγ are present in all compartments of the Purkinje neuron (cell body, axon, and dendrite), localization of cGK1 and GluRδ2 is more prominent in the dendrites and cell body and nearly absent in the Purkinje axons. Already after 16 weeks, a clear decrease in the number of IP3R1 and cGK1 positive cell bodies in KO tissue was observed. An explanation for the seemingly random pattern of affected Purkinje cell bodies was the stochastic nature of DNA damage that did not stress all cells equally. After 26 weeks, the reduction in IP3R1 and cGK1 protein levels was even more eminent, again confirming the proteomics results. Note the increase in Calbindin, IP3R1, and PKCγ in the few remaining Purkinje cells at 26 weeks.

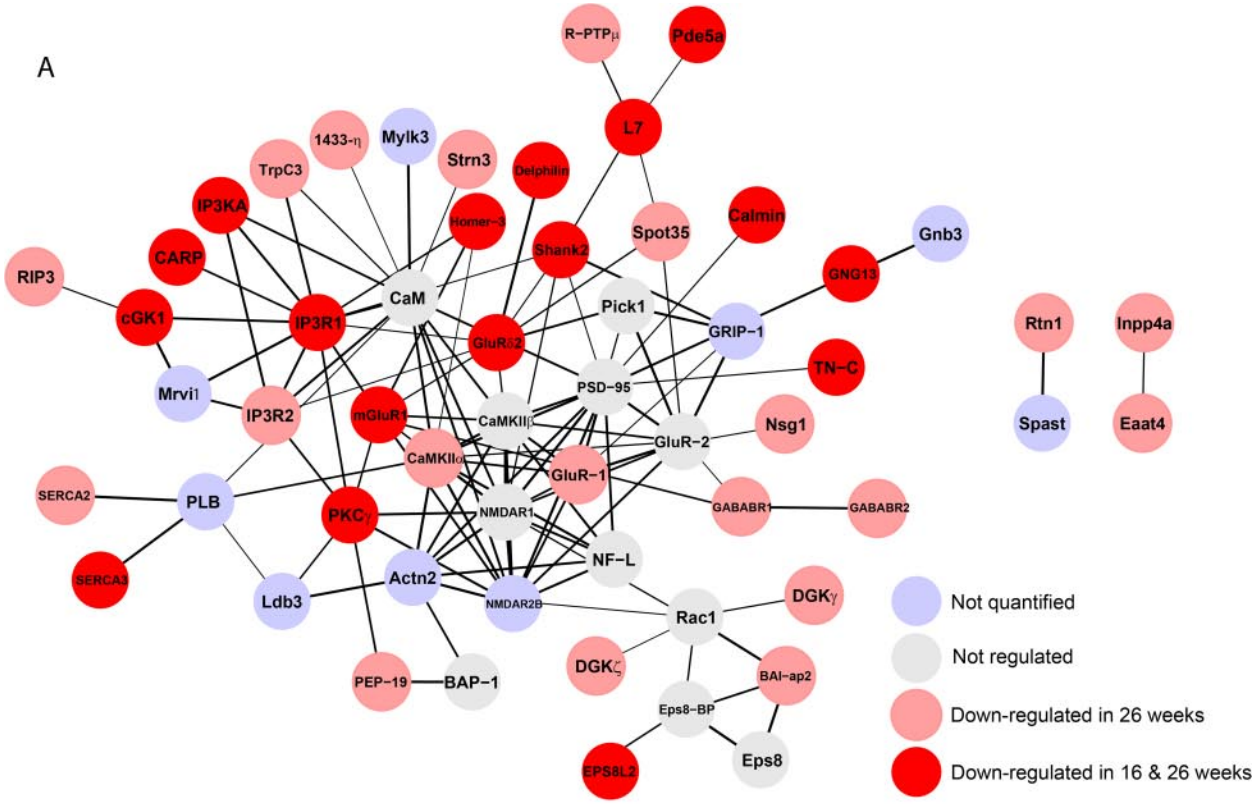

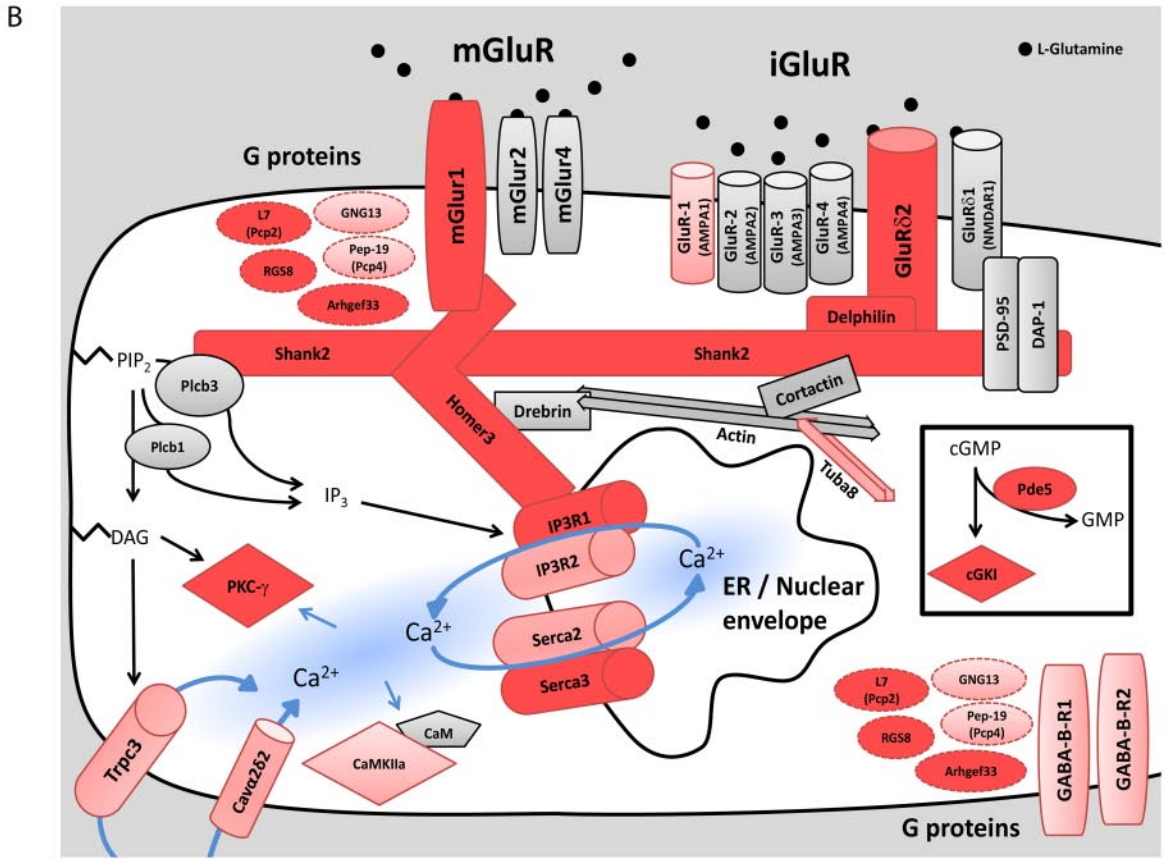

Although Calbindin and IP3R1 are still partly present in Purkinje cell bodies and the molecular layer, a near complete absence of cGK1 was observable. In contrast, although the PKCγ staining shows a clear reduction of axon numbers and a strong shrinkage of most Purkinje cells, PKCγ is still present after 26 weeks. In summary, this indicates that there is a strong effect of DNA damage on neuronal morphology. As the functions of neurons are heavily dependent on its structural contact and communication with other neurons, it is clear that the observed morphological changes will also affect Purkinje neuron functions.

As mentioned above, a strong reduction of several Purkinje markers (L7, PEP-19, and Calbindin) was observed. The down-regulation of these markers can be explained in different ways. One simple explanation could be that Purkinje cells with defects in its DNA-repair machinery contain a high amount of DNA damage, and therefore, the cells will enter apoptosis and disappear. An alternative explanation could be that DNA damage results in a compromise of neuronal cell functioning inducing morphological and functional changes of the affected Purkinje cells. In the second case, the loss of Purkinje markers could indicate the loss of Purkinje characteristic functions rather than cell death/depletion. To test these two hypothesizes, the rate of apoptosis was monitored using staining for activated caspase-3. In addition, GFAP, Galectin-3 (Mac-2), and silver stainings were performed to visualize neuronal inflammation, phagocytosing macrophages, and neuronal degeneration, respectively.

The protein stainings confirmed the up-regulation of caspase-3, GFAP, and Galectin-3 in Purkinje-specific *Ercc1*$^{f/-}$ cerebella as found by the proteomics screening (Fig. 4, Table I, and supplemental Fig. S3). In addition, IHC revealed that DNA damage induced a strong localization of caspase-3 toward the molecular layer, suggesting a strong negative effect of DNA damage on dendrite synapse maintenance. It has indeed been reported previously that high caspase activity in dendrites could be responsible for synaptic breakdown and plasticity (28). The dendrite retraction in Purkinje-specific *Ercc1* KO mice is further supported by an increase in inflammation in the molecular layer, measured by the up-regulation of the astrocyte markers GFAP and Cx-43 (Table I, Fig. 4, and supplemental Figs. S4 and S5*B*). Furthermore, as a result of these changes, the thickness of the molecular layer of the *Ercc1* KO cerebella is significantly decreased when compared with control tissues (supplemental Fig. S6). When looking at phagocytosing macrophages (Mac-2 staining) and degenerative tissue (as indicated by the silver stain), there is a strong almost exclusive increase in the white matter layer of *Ercc1*$^{f/-}$ mice (Fig. 4). The white matter layer is made up largely of myelinated nerve fibers running to and from the cortex, including Purkinje axons (Fig. 3 and supplemental Fig. S7). The neurodegenerative staining could possibly indicate a less controlled retraction of Purkinje axons, resulting in the rejection of dead axon structures that need to be cleared by macrophages. In summary, the IHC stainings confirmed a molecular neurodegenerative phenotype of the cerebellum matching to the behavioral phenotype, mimicking aspects of aging. In addition, the staining indicated different mechanisms could be involved in Purkinje axon and dendrite breakdown, respectively.

DISCUSSION

The link between DNA damage and aging (2) has been firmly associated in different organs (1), including the brain (26, 30). Moreover, genetic defects in genome maintenance and DNA-repair pathways are responsible for multiple premature symptoms of aging (31). Therefore, the study of these progeroid syndromes can shed light on the molecular mechanisms behind the process of aging.

In this study, a cell type-specific Ercc1 KO was used to screen for molecular changes in aged cerebella. From time course experiments, it was clear that DNA damage in Purkinje neurons primarily affect the synaptic areas. Both our proteomics screening and immunohistochemistry stainings showed a decrease in synaptic protein levels. These proteins include neurotransmitter receptors (*i.e.* GluRδ2 and mGluR1), signaling molecules (*i.e.* PKCy and cGK1), and receptor-signal transduction scaffolds (*i.e.* Homer-3 and Delphilin) (Fig. 5). Several proteins involved in synaptic signaling were found to be the first to be affected and regulated after 16 weeks of aberrant DNA repair. Interestingly, at the age of 16 weeks, mice bearing a defective DNA-repair system in Purkinje cells were found to have impaired motor function.[2] In addition to an increase in impaired motor function, the capacity for motoric learning was found to be decreased after 26 weeks. The proteomics data suggest that this may be associated with a strong down-regulation of a large number of synaptic proteins encompassing synaptic protein networks (Fig. 5). In addition, the immunohistochemistry data allowed us to visualize the neuron structure and its protein localization, revealing a strong retraction of proteins from synaptic areas (both dendrites and axons). As a result of this, a drastic morphological change of the affected Purkinje cells was observed.

FIG. 5. **Effect of DNA damage on synaptic signaling protein networks.** *A,* very densely interconnected protein interaction network was calculated by submitting all down-regulated proteins to the STRING database (Heidelberg, Germany). Interactions of higher confidence are indicated by *thicker lines*. *B,* illustration of possible protein interactions/pathways that have been reported in literature, which potentially can occur in Purkinje cells. The *dotted outlined* proteins are placed near G-protein-coupled receptors to show their hypothetical interaction with the receptors and their downstream signaling proteins. Both metabotropic (*mGluR*) and ionotropic (*iGluR*) up- and downstream synaptic signaling pathways display a strong sensitivity for DNA damage.

As proteins are more actively transcribed, their gene locus becomes less structured and more vulnerable to DNA-damaging processes (*i.e.* oxidative stress and random errors). The lack of an efficient nucleotide excision repair pathway therefore sensitizes the areas of the genome that are most actively transcribed. It is known that the maintenance of synapse plasticity requires gene expression and *de novo* protein synthesis; therefore, in retrospect, the down-regulation of synaptic proteins in Ercc1 KO Purkinje cells is not unexpected. Furthermore, the loss of protein expression in strongly affected Purkinje cells was in some cases potentially compensated by neighboring less affected Purkinje cells that seemed to, in response, express the same synaptic proteins to a higher degree (Fig. 3, IP3R1). These microscopic regulations could not be deduced from the high throughput proteomics data or Western blot validation, as in these experiments the protein levels are averaged out over all cells present in the cerebellum, indicating the two applied techniques are complementary.

Our results indicate that DNA damage does not result in direct Purkinje cell removal but gradual functional decline and tissue degeneration. Although a set of Purkinje-specific markers are depleted in the DNA repair-defective Purkinje cells (Table I), the localization of PKCγ (Fig. 3) illustrates that DNA-repair knock-out Purkinje cell bodies have not all disappeared, but at least some have drastically changed their morphology and protein localization. The increased reduction of Purkinje markers over time therefore indicates the functional decline upon increasing amounts of DNA damage. The loss of neuronal functions is in line with previous reports studying aging mechanisms that showed a decrease in neuronal signal processing capabilities (32), reduction of the post-synaptic density (33), and a reduced number of synapses (34) in aged rats.

Finally, in addition to the resemblance with the aging phenotype, the results presented here could potentially shed some light on the development of motoric diseases such as spinocerebellar ataxia. IP3R1, mGluR1, $Ca_v\alpha2\delta2$, and PKC-γ gene mutations are responsible for different types of spinocerebellar ataxia, and considering the motoric impairment of our model system and the strong regulation of these proteins, the list of regulated proteins could also be used as an extended target list to study cerebellar motor diseases, such as ataxia.

* This work was supported, in whole or in part, by National Institutes of Health Grants 1PO1 AG-17242-02 from the National Institute of Aging and Grant 1UO1 ES011044 from the NIEHS. This work was also supported by The Netherlands Proteomics Centre, The Netherlands Genomics Initiative, and the Centre for Biomedical Genetics. This work was also supported in part by the PRIME-XS Project, Grant Agreement 262067, funded by the European Union Seventh Framework Program; the European Commission FP7 Markage Grant FP7-Health-2008-200880; DNA Repair Grant LSHG-CT-2005-512113 and LifeSpan Grant LSHG-CT-2007-036894; the Royal Academy of Arts and Sciences of the Netherlands (academia professorship to J.H.J.H.), and a European Research Council Advanced Grant to J.H.J.H. The research leading to these results has received funding from the European Community's Seventh Framework Programme FP7/2007-2013 under Grant Agreement HEALTH-F2-2010-259893.

[S] This article contains supplemental material.

§§ To whom correspondence may beaddressed: Tel. nr.: 0031302535871 Fax nr.: 0031302536919 E-mail: a.j.r.heck@uu.nl or E-mail: m.altelaar@uu.nl.

REFERENCES

1. Hoeijmakers, J. H. (2009) DNA damage, aging, and cancer. *N. Engl. J. Med.* **361,** 1475–1485
2. Wang, J., Clauson, C. L., Robbins, P. D., Niedernhofer, L. J., and Wang, Y. (2012) The oxidative DNA lesions 8,5′-cyclopurines accumulate with aging in a tissue-specific manner. *Aging Cell.,* **11,** 714–716
3. Kyng, K. J., and Bohr, V. A. (2005) Gene expression and DNA repair in progeroid syndromes and human aging. *Ageing Res. Rev.* **4,** 579–602
4. McWhir, J., Selfridge, J., Harrison, D. J., Squires, S., and Melton, D. W. (1993) Mice with DNA repair gene (ERCC-1) deficiency have elevated levels of p53, liver nuclear abnormalities and die before weaning. *Nat. Genet.* **5,** 217–224
5. Weeda, G., Donker, I., de Wit, J., Morreau, H., Janssens, R., Vissers, C. J., Nigg, A., van Steeg, H., Bootsma, D., and Hoeijmakers, J. H. (1997) Disruption of mouse ERCC1 results in a novel repair syndrome with growth failure, nuclear abnormalities, and senescence. *Curr. Biol.* **7,** 427–439
6. Niedernhofer, L. J., Garinis, G. A., Raams, A., Lalai, A. S., Robinson, A. R., Appeldoorn, E., Odijk, H., Oostendorp, R., Ahmad, A., van Leeuwen, W., Theil, A. F., Vermeulen, W., van der Horst, G. T., Meinecke, P., Kleijer, W. J., Vijg, J., Jaspers, N. G., and Hoeijmakers, J. H. (2006) A new progeroid syndrome reveals that genotoxic stress suppresses the somatotroph axis. *Nature* **444,** 1038–1043
7. Lawrence, N. J., Sacco, J. J., Brownstein, D. G., Gillingwater, T. H., and Melton, D. W. (2008) A neurological phenotype in mice with DNA repair gene Ercc1 deficiency. *DNA Repair* **7,** 281–291
8. Végh, M. J., de Waard, M. C., van der Pluijm, I., Ridwan, Y., Sassen, M. J., van Nierop, P., van der Schors, R. C., Li, K. W., Hoeijmakers, J. H., Smit, A. B., and van Kesteren, R. E. (2012) Synaptic proteome changes in a DNA repair-deficient ercc1 mouse model of accelerated aging. *J. Proteome Res.* **11,** 1855–1867
9. Schrimpf, S. P., Meskenaite, V., Brunner, E., Rutishauser, D., Walther, P., Eng, J., Aebersold, R., and Sonderegger, P. (2005) Proteomic analysis of synaptosomes using isotope-coded affinity tags and mass spectrometry. *Proteomics* **5,** 2531–2541
10. Nielsen, P. A., Olsen, J. V., Podtelejnikov, A. V., Andersen, J. R., Mann, M., and Wisniewski, J. R. (2005) Proteomic mapping of brain plasma membrane proteins. *Mol. Cell. Proteomics* **4,** 402–408
11. Coughenour, H. D., Spaulding, R. S., and Thompson, C. M. (2004) The synaptic vesicle proteome: a comparative study in membrane protein identification. *Proteomics* **4,** 3141–3155
12. Cheng, D., Hoogenraad, C. C., Rush, J., Ramm, E., Schlager, M. A., Duong, D. M., Xu, P., Wijayawardana, S. R., Hanfelt, J., Nakagawa, T., Sheng, M., and Peng, J. (2006) Relative and absolute quantification of postsynaptic density proteome isolated from rat forebrain and cerebellum. *Mol. Cell. Proteomics* **5,** 1158–1170
13. Barski, J. J., Dethleffsen, K., and Meyer, M. (2000) Cre recombinase expression in cerebellar Purkinje cells. *Genesis* **28,** 93–98
14. Doig, J., Anderson, C., Lawrence, N. J., Selfridge, J., Brownstein, D. G., and Melton, D. W. (2006) Mice with skin-specific DNA repair gene (Ercc1) inactivation are hypersensitive to ultraviolet irradiation-induced skin cancer and show more rapid actinic progression. *Oncogene* **25,** 6229–6238
15. Boersema, P. J., Raijmakers, R., Lemeer, S., Mohammed, S., and Heck, A. J. (2009) Multiplex peptide stable isotope dimethyl labeling for quantitative proteomics. *Nat. Protoc.* **4,** 484–494
16. Gauci, S., Helbig, A. O., Slijper, M., Krijgsveld, J., Heck, A. J., and Mohammed, S. (2009) Lys-N and trypsin cover complementary parts of the phosphoproteome in a refined SCX-based approach. *Anal. Chem.* **81,** 4493–4501
17. Roxas, B. A., and Li, Q. (2008) Significance analysis of microarray for relative quantitation of LC/MS data in proteomics. *BMC Bioinformatics* **9,** 187

18. Dahlhaus, M., Li, K. W., van der Schors, R. C., Saiepour, M. H., van Nierop, P., Heimel, J. A., Hermans, J. M., Loos, M., Smit, A. B., and Levelt, C. N. (2011) The synaptic proteome during development and plasticity of the mouse visual cortex. *Mol. Cell. Proteomics* **10,** M110 005413
19. Munoz, J., Low, T. Y., Kok, Y. J., Chin, A., Frese, C. K., Ding, V., Choo, A., and Heck, A. J. (2011) The quantitative proteomes of human-induced pluripotent stem cells and embryonic stem cells. *Mol. Syst. Biol.* **7,** 550
20. Tusher, V. G., Tibshirani, R., and Chu, G. (2001) Significance analysis of microarrays applied to the ionizing radiation response. *Proc. Natl. Acad. Sci. U.S.A.* **98,** 5116–5121
21. Jaarsma, D., Haasdijk, E. D., Grashorn, J. A., Hawkins, R., van Duijn, W., Verspaget, H. W., London, J., and Holstege, J. C. (2000) Human Cu/Zn superoxide dismutase (SOD1) overexpression in mice causes mitochondrial vacuolization, axonal degeneration, and premature motoneuron death and accelerates motoneuron disease in mice expressing a familial amyotrophic lateral sclerosis mutant SOD1. *Neurobiol. Dis.* **7,** 623–643
22. Nadler, J. V., and Evenson, D. A. (1983) Use of excitatory amino acids to make axon-sparing lesions of hypothalamus. *Methods Enzymol.* **103,** 393–400
23. de Waard, M. C., van der Pluijm, I., Zuiderveen Borgesius, N., Comley, L. H., Haasdijk, E. D., Rijksen, Y., Ridwan, Y., Zondag, G., Hoeijmakers, J. H., Elgersma, Y., Gillingwater, T. H., and Jaarsma, D. (2010) Age-related motor neuron degeneration in DNA repair-deficient Ercc1 mice. *Acta Neuropathol.* **120,** 461–475
24. Walther, D. M., and Mann, M. (2011) Accurate quantification of more than 4000 mouse tissue proteins reveals minimal proteome changes during aging. *Mol. Cell. Proteomics* **10,** M110 004523
25. Borgesius, N. Z., de Waard, M. C., van der Pluijm, I., Omrani, A., Zondag, G. C., van der Horst, G. T., Melton, D. W., Hoeijmakers, J. H., Jaarsma, D., and Elgersma, Y. (2011) Accelerated age-related cognitive decline and neurodegeneration, caused by deficient DNA repair. *J. Neurosci.* **31,** 12543–12553
26. Lu, T., Pan, Y., Kao, S. Y., Li, C., Kohane, I., Chan, J., and Yankner, B. A. (2004) Gene regulation and DNA damage in the ageing human brain. *Nature* **429,** 883–891
27. Penkowa, M., Carrasco, J., Giralt, M., Moos, T., and Hidalgo, J. (1999) CNS wound healing is severely depressed in metallothionein I- and II-deficient mice. *J. Neurosci.* **19,** 2535–2545
28. Gilman, C. P., and Mattson, M. P. (2002) Do apoptotic mechanisms regulate synaptic plasticity and growth-cone motility? *Neuromolecular Med.* **2,** 197–214
29. Jacobs, B., Driscoll, L., and Schall, M. (1997) Life-span dendritic and spine changes in areas 10 and 18 of human cortex: a quantitative Golgi study. *J. Comp. Neurol.* **386,** 661–680
30. Esiri, M. M. (2007) Ageing and the brain. *J. Pathol.* **211,** 181–187
31. Garinis, G. A., van der Horst, G. T., Vijg, J., and Hoeijmakers, J. H. (2008) DNA damage and ageing: new-age ideas for an age-old problem. *Nat. Cell Biol.* **10,** 1241–1247
32. Deupree, D. L., Bradley, J., and Turner, D. A. (1993) Age-related alterations in potentiation in the CA1 region in F344 rats. *Neurobiol. Aging* **14,** 249–258
33. Nicholson, D. A., Yoshida, R., Berry, R. W., Gallagher, M., and Geinisman, Y. (2004) Reduction in size of perforated postsynaptic densities in hippocampal axospinous synapses and age-related spatial learning impairments. *J. Neurosci.* **24,** 7648–7653
34. Geinisman, Y., deToledo-Morrell, L., Morrell, F., Persina, I. S., and Rossi, M. (1992) Age-related loss of axospinous synapses formed by two afferent systems in the rat dentate gyrus as revealed by the unbiased stereological dissector technique. *Hippocampus* **2,** 437–444